Article

In Vitro Anti-Proliferative and Apoptotic Effects of Hydroxytyrosyl Oleate on SH-SY5Y Human Neuroblastoma Cells

Valentina Laghezza Masci [1], Roberta Bernini [2,*], Noemi Villanova [2], Mariangela Clemente [2], Vittoria Cicaloni [3], Laura Tinti [3], Laura Salvini [3], Anna Rita Taddei [4], Antonio Tiezzi [1] and Elisa Ovidi [1]

[1] Department for Innovation in Biological, Agro-Food and Forest Systems (DIBAF), University of Tuscia, Largo dell'Università, 01100 Viterbo, Italy
[2] Department of Agriculture and Forest Sciences (DAFNE), University of Tuscia, Via San Camillo de Lellis snc, 01100 Viterbo, Italy
[3] Toscana Life Science Foundation, Via Fiorentina 1, 53100 Siena, Italy
[4] High Equipment Centre, Tuscia University, Largo dell'Università snc, 01100 Viterbo, Italy
* Correspondence: roberta.bernini@unitus.it

Abstract: The antitumor activity of polyphenols derived from extra virgin olive oil and, in particular the biological activity of HTyr, has been studied extensively. However, the use of HTyr as a therapeutic agent for clinical applications is limited by its low bioavailability and rapid excretion in humans. To overcome these limitations, several synthetic strategies have been optimized to prepare lipophenols and new compounds derived from HTyr to increase lipophilicity and bioavailability. One very promising ester is hydroxytyrosyl oleate (HTyr-OL) because the chemical structure of HTyr, which is responsible for several biological activities, is linked to the monounsaturated chain of oleic acid (OA), giving the compound high lipophilicity and thus bioavailability in the cellular environment. In this study, the in vitro cytotoxic, anti-proliferative, and apoptotic induction activities of HTyr-OL were evaluated against SH-SY5Y human neuroblastoma cells, and the effects were compared with those of HTyr and OA. The results showed that the biological activity of HTyr was maintained in HTyr-OL treatments at lower dosages. In addition, the shotgun proteomic approach was used to study HTyr-OL-treated and untreated neuroblastoma cells, revealing that the antioxidant, anti-proliferative and anti-inflammatory activities of HTyr-OL were observed in the unique proteins of the two groups of samples.

Keywords: plant-derived compounds; hydroxytyrosol; hydroxytyrosol oleate; SH-SY5Y human neuroblastoma cells; cytotoxicity; anti-proliferative activity; apoptosis induction activity

1. Introduction

The biological activities of natural substances have been exploited since ancient times and have been used to treat various human diseases [1]. The relevant anti-tumor properties of some plant molecules and semi-synthetic or synthetic analogues are well studied and are used against several types of cancer today [2–4].

Hydroxytyrosol (3,4-dihydroxyphenethyl alcohol, HTyr, Figure 1) is a low-molecular-weight and amphiphilic phenol found in the fruit of the olive tree (*Olea europaea* L.), a plant widely cultivated in Spain, Italy, Greece, and Turkey either for the consumption of table olives or to produce extra-virgin olive oil (EVOO).
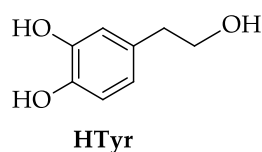
Figure 1. Chemical structure of hydroxytyrosol (HTyr).

EVOO represents a key component of the Mediterranean diet, a dietary regime which recommends the daily intake of vegetables, fruits, grains, legumes, and nuts for a healthy lifestyle and to prevent the onset of cardiovascular diseases, cancer, type 2 diabetes, neurodegenerative disorders, and aging [5,6]. These foods are rich in active ingredients, including phenolic compounds, which are responsible for their beneficial effects on human health [7,8].

During olive ripening and EVOO production, the content of HTyr in fruit increases due to the hydrolytic activity of an endogenous β-glucosidase on oleuropein, a secoiridoid derivative, giving rise to HTyr, elenolic acid, and glucose [9].

Both oleuropein and HTyr can be recovered from olive oil by-products by innovative and eco-friendly technologies, according to the modern "circular economy strategy", in which waste from one production process represents the raw materials for a new process [10]. Oleuropein can be extracted from olive leaves, a solid waste derived mainly from the pruning of olive trees, while HTyr can be recovered from liquid (olive oil wastewaters) and solid (pomace) wastes produced during EVOO processing [11,12].

In vitro experiments have evidenced that HTyr is not genotoxic and mutagenic at concentrations corresponding to the daily consumption of EVOO [13]. In vivo studies have shown that HTyr does not induce effects of toxicological significance even at high doses with a proposed NOAL (No Observed Adverse Effect Level) of 500 mg/kg/d [14].

HTyr displays a variety of biological activities [15], including antioxidant [16], anti-inflammatory [17], anticancer [18–20], anti-diabetic [21], cardioprotective [22], and neuroprotective [23,24] properties. Recent studies have evidenced that HTyr plays a relevant role in the prevention of neurodegenerative diseases [25], in the neurogenesis of adult and aged mice and in increasing the survival of new neurons [26].

For all its described properties, HTyr has been granted the Generally Recognized as Safe (GRAS) designation by the United States Food and Drug Administration (FDA), and is a precious ingredient for nutraceutical, cosmeceutical, and food formulations [13].

For its content in the EVOO, the European Food Safety Authority (EFSA) has approved a health claim which states that "olive oil polyphenols contribute to the protection of blood lipids from oxidative stress". However, this effect is observed only with a daily intake of 20 g of an olive oil "containing at least 5 mg of hydroxytyrosol and its derivatives (e.g., oleuropein complex and tyrosol)" [27].

Despite both its excellent safety profile and strong biological activities, the use of HTyr as a therapeutic agent for clinical applications is limited by its low bioavailability and fast excretion in humans [28].

To overcome these limitations, a variety of synthetic strategies have been optimized to prepare lipophenols as HTyr esters [29–32], HTyr ethers [33–35], and new HTyr-derived compounds [36–38].

Among them, HTyr alkyl esters are the most studied compounds. Structurally, they are characterized by the catecholic moiety, as well as an alkyl chain linked by an ester bond on the alcoholic functionality. The chain length allows for modulation of the lipophilicity, a property that modifies the bioavailability of a molecule in the cellular environment and its solubility in non-aqueous media as oils and emulsions [32,39].

A very promising ester is hydroxytyrosyl oleate (HTyr-OL), a compound characterized by a high lipophilicity due to the presence of the C18 monounsaturated chain of oleic acid (OA, Figure 2). Recently, HTyr-OL has been identified in EVOO and olive oil by-products,

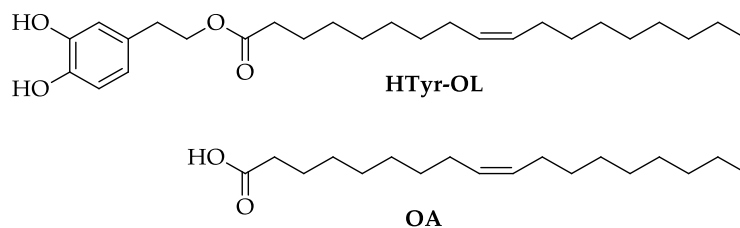while it has been found to be absent in olives, suggesting that it is obtained during oil production [40].

Figure 2. Chemical structure of hydroxytyrosyl oleate (HTyr-OL) and oleic acid (OA).

In recent years, HTyr-OL has aroused interest; however, only a few studies have been published to date. HTyr-OL has shown an anti-proliferative effect on the human colon cancer cell line HCT8-β8, engineered to overexpress oestrogen receptor β (ERβ) [41]; exhibited anti-inflammatory activity by reducing nitric oxide production by lipopolysaccharide-stimulated RAW264.7 macrophages [40]; antioxidant activity in human keratinocytes [42]; anti-diabetic properties by inducing insulin secretion in pancreatic cell line 832/13 [43].

To the best of our knowledge, no studies have yet been conducted on the effects of HTyr-OL on the SH-SY5Y human neuroblastoma cell line. Neuroblastoma is a pediatric cancer arising from neural progenitor cells with a very high biological and clinical heterogeneity [44].

Due to the lack of literature, the aim of this investigation was to evaluate the in vitro cytotoxicity, anti-proliferative, and apoptotic induction activities of HTyr-OL against SH-SY5Y human neuroblastoma cells, and to then compare these effects to those of HTyr and OA separately. The cell viability assays were followed by Western blot, flow cytometry, electron microscopy and proteomic techniques. The proteomic approach was applied downstream to analyse the cellular pathways involved in the response to HTyr-OL treatment.

2. Results

2.1. Synthesis of HTyr and HTyr-OL

HTyr was synthetized according to a procedure already reported in the literature [45], with some modifications. Briefly, tyrosol (4-hydroxyphenethyl alcohol) was oxidized with 2-iodoxybenzoic acid [1-hydroxy-1-oxo-1H-1λ5- benz[d][1,2]iodoxol-3-one, IBX] [46] in methanol and then treated with sodium dithionite ($Na_2S_2O_4$) in water. After chromatographic purification, HTyr was isolated in 40% yield (Scheme 1).
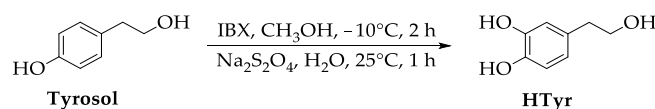
Scheme 1. Synthesis of HTyr.

HTyr-OL was obtained by esterification of HTyr with oleyl chloride in dimethyl carbonate (DMC), as depicted in Scheme 2. HTyr-OL was isolated in a 60% yield [32].
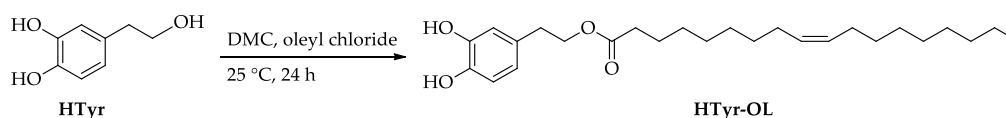
Scheme 2. Synthesis of HTyr-OL.

2.2. Cytotoxic Activity

The cytotoxic effect of HTyr-OL, HTyr and OA on SH-SY5Y cells was evaluated using the MTT assay, and cell viability was measured after 72 h of treatment. The results showed that HTyr-OL had a stronger dose-dependent effect on neuroblastoma cells than HTyr and OA (Figure 3a).
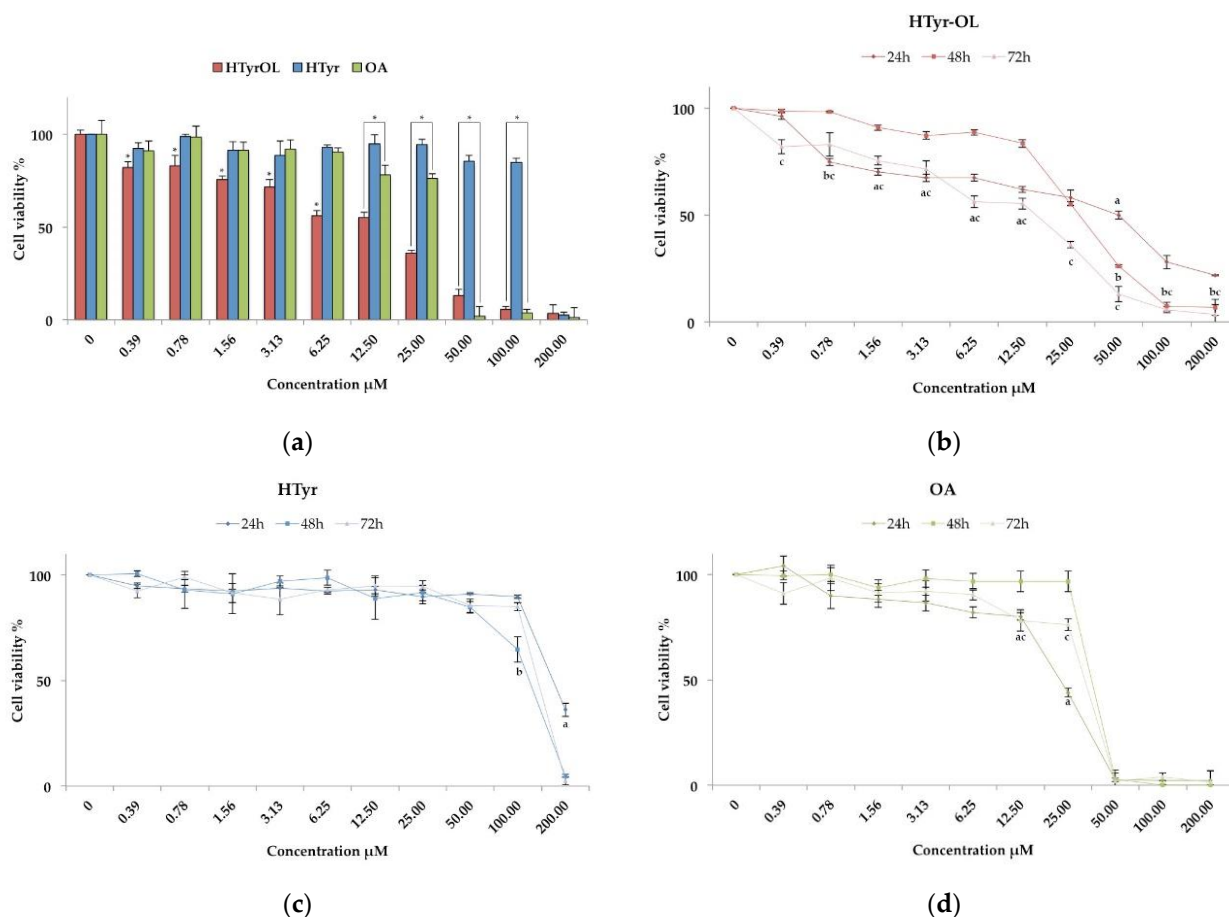

(**a**)

(**b**)

(**c**)

(**d**)

Figure 3. (**a**) Graph bar of cytotoxic activity. The cell viability percentages of SH-SY5Y are plotted against treatment concentrations; (**b**) Line graphs of the anti-proliferative effects of HTyr-OL, (**c**) HTyr, and (**d**) OA on SH-SY5Y neuroblastoma cells at 24, 48, and 72 h. Results are expressed as mean of cell viability against concentration (μM). The values are expressed as % $\pm$ SD. *, *p*-value < 0.05 significant differences compared with ctrl group; a, *p*-value < 0.05 significant differences compared with 48 and 72 h; b, *p*-value < 0.05 significant differences compared with 24 and 72 h; c, *p*-value < 0.05 significant differences compared with 24 and 48 h.

After 72 h of exposure to the treatments, by comparing the half maximal effective concentration (EC_{50}) values obtained for SH-SY5Y cells, the activity of HTyr-OL was found to be stronger than that of HTyr. The EC_{50} value of HTyr, 114.02 $\pm$ 1.69 μM, was about four times higher than that of HTyr-OL, 26.35 $\pm$ 3.75 μM. The OA-treated cells responded with an EC_{50} value of 35.93 $\pm$ 3.57 μM.

To assess whether the observed cytotoxic activity may be selective on tumor cells, normal human cell lines (MCF10A) were treated as the SH-SY5Y cells; EC_{50} values above 200 μM were obtained for all three compounds (Table 1), thus confirming a more selective affection of HTyr-OL to the neuroblastoma cell model.

Table 1. HTyr-OL, HTyr, and OA EC_{50} values against SH-SY5Y and MCF10A cells.

Compound	EC$_{50}$ (µM Mean ± SD)	
	SH-SY5Y	MCF10A
HTyr-OL	26.35 ± 3.75 [a]	>200
HTyr	114.02 ± 1.69	>200
OA	35.93 ± 3.57 [b]	>200

[a] $p < 0.05$ significant differences compared with HTyr and OA treated groups. [b] $p < 0.05$ significant differences compared with HTyr and HTyr-OL treated groups.

2.3. Anti-Proliferative Effect

The anti-proliferative effects of HTyr-OL, HTyr, and OA were studied by measuring the mitochondrial dehydrogenase activity as an indicator of the cell viability (MTT assay) of SH-SY5Y cells after 24, 48, and 72 h of treatment exposure. HTyr-OL demonstrated dose- and time-dependent effects on neuroblastoma cells (Figure 3b), while HTyr and OA showed dose-dependent and non-time-dependent effects (Figure 3c,d). This evidence was also provided by the EC_{50} values obtained.

As depicted in Table 2, the EC_{50} values of HTyr-OL decreased by about half as the treatment time increased from 24 to 48 h, ranging from 48.97 ± 9.04 µM to 27.76 ± 2.31 µM. The growth inhibition obtained at 48 h was maintained at 72 h, whereas the EC_{50} values showed no significant change.

Table 2. HTyr-OL, HTyr, and OA EC_{50} values against SH-SY5Y after 24, 48 and 72 h of treatment.

Compound	EC$_{50}$ (µM Mean ± SD)		
	24 h	48 h	72 h
HTyr-OL	48.97 ± 9.04 [a]	27.76 ± 2.31 [b]	26.35 ± 3.75 [b]
HTyr	150.13 ± 7.89	113.59 ± 7.87	114.02 ± 1.69
OA	36.91 ± 4.93 [a]	38.64 ± 5.28 [c]	35.93 ± 3.57 [c]

[a] p-value < 0.05 significant differences compared with HTyr treated group. [b] p-value < 0.05 significant differences compared with HTyr and OA treated groups. [c] p-value < 0.05 significant differences compared with HTyr and HTyr-OL treated groups.

2.4. Apoptosis Detection by Flow Cytometry

The cytotoxic and anti-proliferative effects observed following treatments with HTyr-OL, HTyr, and OA were further investigated to determine whether cell death was related to an apoptotic process. Neuroblastoma cells were treated for 24 h with EC_{50} doses of the tested compounds and processed for flow cytometry, with the presence of Annexin V-FITC and Propidium Iodide (PI) being analyzed (Figure 4).

The cells treated with HTyr-OL and OA showed similar apoptotic rate percentages, 52.36% ± 4.31% and 49.91% ± 6.94%, respectively, corresponding to the sum of the percentage of Annexin V-positive/PI-negative stained (early apoptosis) and Annexin V-positive/PI-positive (late apoptosis) stained cells. The highest apoptotic rate was found for the HTyr-treated cells (79.64% ± 8.83%), with a value close to that of vinblastine treated (VBL treated) cells (74.24% ± 6.29%) obtained (Table 3).
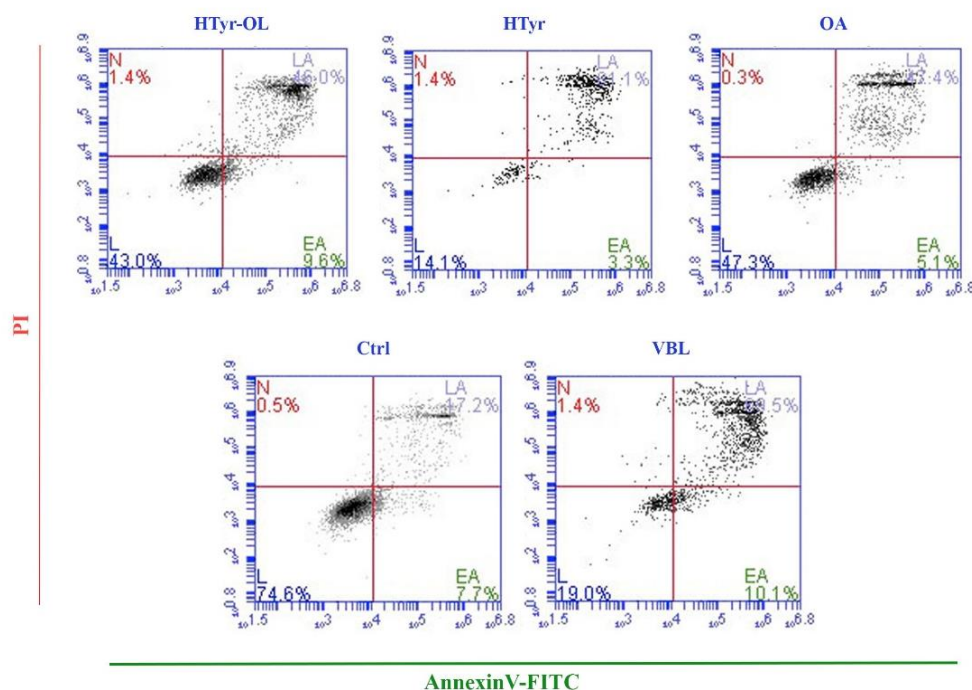
Figure 4. Apoptosis detection by flow cytometry. Flow cytometric analysis of the HTyr-OL, HTyr and OA treatments on SH-SY5Y cells for apoptosis determination using AnnexinV-FITC/PI staining. L: live cells; EA: early apoptotic cells; LA: late apoptotic cells; N: necrotic cells.

Table 3. Apoptotic rate percentages obtained from the sum of the percentages of EA and LA cells. The values are expressed as % ± standard error mean. *p*-value < 0.05 significant differences compared with Ctrl group.

Compound	Apoptotic Rate %
HTyr-OL	52.36 ± 4.31
HTyr	79.64 ± 8.83
OA	49.91 ± 6.94
Ctrl	22.25 ± 2.69
VBL	74.24 ± 6.29

2.5. Scanning Electron Microscopy Investigation

To define the morphological changes following the treatments with HTyr-OL, HTyr, and OA in SH-SY5Y cells, scanning electron microscopy was performed. Treatment with HTyr-OL resulted in a change in cell morphology, with the appearance of spherical-shaped cells and subsequent loss of cell adhesion observed (Figure 5a). The morphologically altered cells were characterized by surface changes, with the presence of protrusions and blebs observed. The same conditions at the plasma membrane level were found in HTyr and OA treated cells (Figure 5b,c), in which no rounded cells with a loss of adhesion were detected. In Figure 5d, Ctrl cells are shown that were characterized by a normal morphology, and a regular surface with thin and properly distributed cell protrusions, typical of an adherent cell. In contrast, SH-SY5Y treated with VBL showed typically apoptotic features, with the presence of roundish cells, morphological alterations, and blebs on the surface observed (Figure 5e).
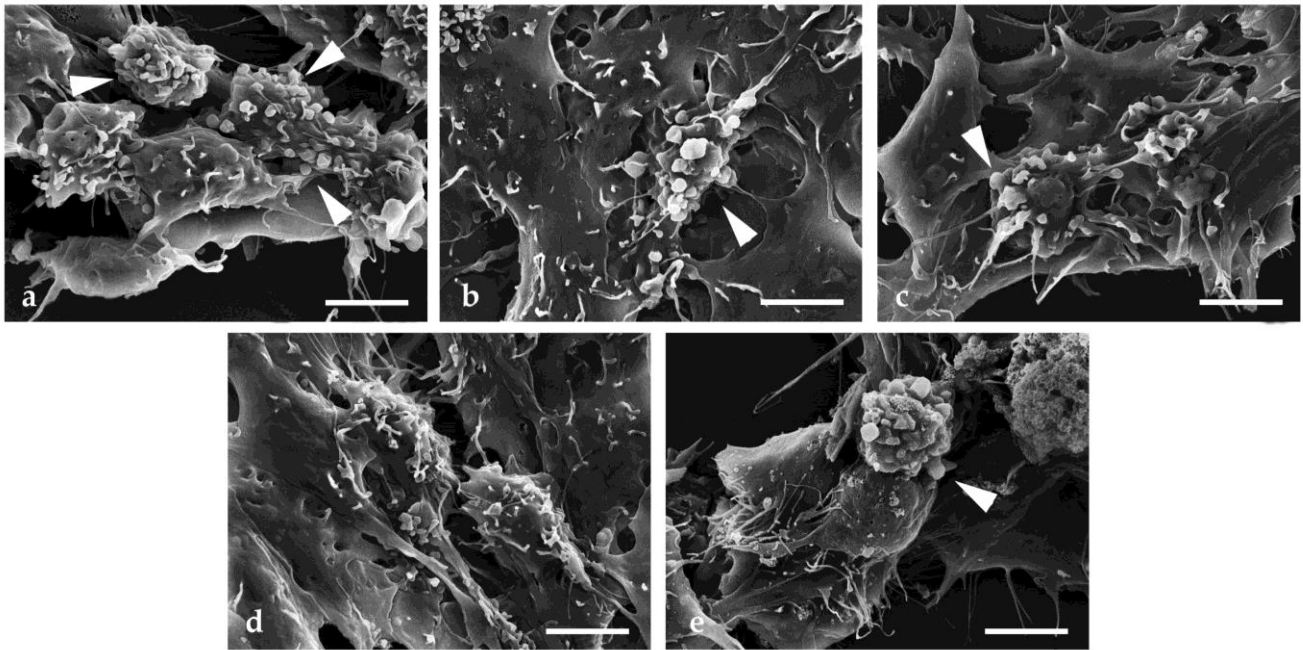
Figure 5. SEM micrographs of SH-SY5Y cells at 24 h of EC$_{50}$ treatments, with: (**a**) HTyr-OL; (**b**) HTyr; (**c**) OA; (**d**) Ctrl or untreated cells; (**e**) VBL. Arrowheads for membrane blebbing of apoptotic cells. Scale bars 5 µm.

2.6. Detection of Caspase-3 Activated by Western Blot

To validate the results obtained by flow cytometry, the presence of activated caspase-3 was detected by immunoblotting techniques. The monoclonal antibody against activated caspase-3 recognized two bands (19 kDa and 17 kDa), corresponding to the major and minor fragments, resulting in the cutting of the amino acid Asp175 in caspase-3.

Figure 6a shows that in HTyr-OL and HTyr-treated samples, both bands were detected, with intensities obtained that were comparable to those of samples treated with apoptosis inducer (VBL). In the lysates obtained in OA-treated cells and untreated cells (Ctrl), very weak bands were detected, the intensity of which was determined by image processing and subsequent quantification (Figure 6b).
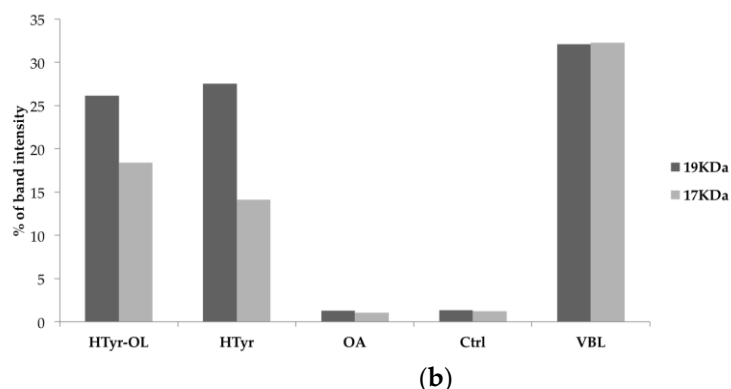

(**a**)

Figure 6. *Cont.*

(b)
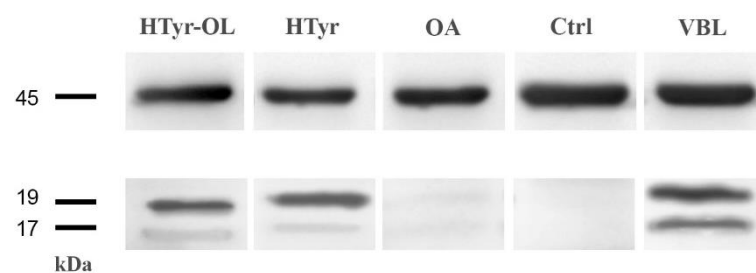
Figure 6. Western blot analysis for expression of cleaved caspase-3, studied using a cleaved caspase-3 monoclonal antibody. (**a**) In the lower panel, the representative image of detection of cleaved caspase-3 in SH-SY5Y cells treated with HTyr-OL, HTyr, OA; Ctrl and VBL cells were negative and positive controls, respectively (one of the three experiments). In the upper panel, detection of β-actin as the internal control; (**b**) Graph bar showing differences in intensity of caspase-3 obtained by pictures in (**a**), quantitatively evaluated using the ImageJ program.

2.7. Shotgun Proteomic Approach and Gene Ontology Functional Annotation

A shotgun proteomic approach was performed to investigate the differential protein expression profile in Ctrl and HTyr-OL samples. A total of 3911 and 3400 proteins were identified in the treatment group (HTyr-OL) and Ctrl group, respectively, deriving from the triplicates of each condition. A total of 3180 unique proteins associated with a known *Homo sapiens* protein were found to be shared by the two sample groups, 220 were unique in HTyr-OL and 731 were unique in the Ctrl group. A numerical comparison was carried out, and this is presented in a Venn diagram (Figure 7a). The "overlap index" based on the Jaccard similarity coefficient (which measures similarity between finite sample sets and is defined as the size of the intersection divided by the size of the union of the sample sets) was 0.77. For the Ctrl group, 18.69% of the total proteome was unique, while 81.31% was shared with HTyr-OL. Similarly, for the HTyr-OL sample, 6.47% of the whole protein dataset was unique, while 93.53% was shared with the Ctrl.

The unique protein lists identified in the Ctrl and HTyr-OL treated groups were subjected to functional annotation analysis. The enriched Gene Ontology (GO) terms in the molecular function (Figure 7b) category showed a significant difference (p-value < 0.001) in favour of Ctrl in GO terms "Transcription regulator activity" (7.0% in Ctrl; 3.3% in HTyr-OL) and "RNA binding" (4.3% in Ctrl; 2.8% in HTyr-OL), whereas the terms "Cell adhesion molecule activity" (0.5% in Ctrl; 3.9% in HTyr-OL) and "Protease inhibitor activity" (0.2% in Ctrl; 2.8% in HTyr-OL) were found to be enriched in HTyr-OL rather than in Ctrl. As far as the cellular component was concerned (Figure 8c), the GO terms "Exosomes" (9.1% in Ctrl; 20.4% in HTyr-OL), "Plasma membrane" (12.0% in Ctrl; 19.8% in HTyr-OL), "Endoplasmic Reticulum" (7.5% in Ctrl; 15.0% in HTyr-OL), "Golgi apparatus" (7.5% in Ctrl; 14.4% in HTyr-OL) and "Extracellular" (6.7% in Ctrl; 13.2% in HTyr-OL) appeared to be significantly enriched GO terms in the HTyr-OL group rather than in Ctrl. In particular, there was a high percentage of unique Ctrl proteins involved in cellular proliferation pathways, such as "Neuroblast proliferation" (67.55% in Ctrl; 32.45% in HTyr-OL), in the inflammation process, such as "Cytokine production involved in inflammatory response" (73.51% in Ctrl; 26.49% in HTyr-OL), "Stress-activated MAPK cascade" (89.28% in Ctrl; 10.72% in HTyr-OL) and "Stress-activated protein kinase signalling cascade" (90.02% in Ctrl; 9.98% in HTyr-OL) and in antioxidant activity, such as "Cellular response to oxidative stress" (60.05% in Ctrl; 39.95% in HTyr-OL).
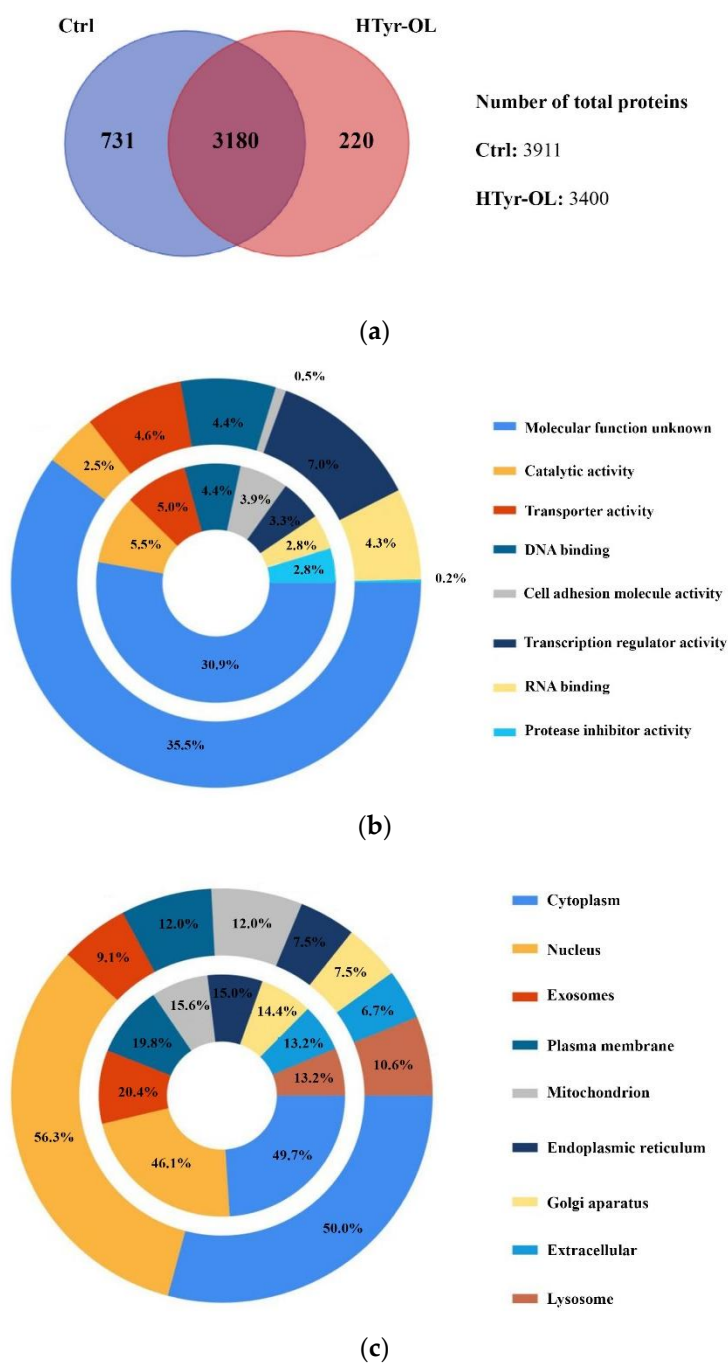
(**a**)

(**b**)

(**c**)

Figure 7. Identified proteins and Gene Ontology analysis. (**a**) Venn diagram representing the number of reproducibly quantified proteins for Ctrl (3911 total proteins) and HTyr-OL (3400 total proteins) samples. (**b**) Molecular functions comparison between Ctrl and HTyr-OL groups. (**c**) Cellular components comparison between Ctrl and HTyr-OL groups. In (**b**,**c**), Ctrl is on the outer chart and HTyr-OL is on the inner chart.

Based on these findings, we investigated also the up/downregulated proteins and specifically selected those involved in apoptosis and proliferation processes. In Figure 8, a Volcano plot comparing the HTyr-OL dataset to the Ctrl dataset is presented; we found a total of 38 statistically significant proteins with up/downregulation. The DEPs identified had ratios higher than 2 and lower than −2, and they were grouped as upregulated and downregulated proteins, respectively. Among these proteins, 17 were found to be upregulated in HTyr-OL and 21 were found to be downregulated (for a complete list, see

Table S1 in Supplementary Materials). These DEPs were then classified into their respective protein classes by mapping them into the Uniprot classification GO system [47] linked with apoptosis and cellular proliferation (five upregulated and two downregulated proteins).
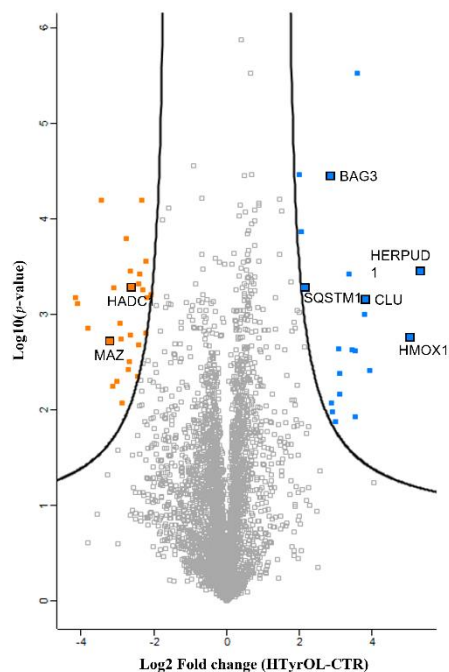

Figure 8. Volcano plot showing proteins differentially expressed in HTyr-OL and Ctrl datasets. Proteins with statistically significant differential expression (S0 = 2, *p*-value > 0.05) are in the top, right and left, quadrants. Upregulated proteins in HTyr-OL are represented in blue; downregulated proteins in HTyr-OL are in orange.

Protein–Protein Interaction Network

The up- and downregulated protein DEPs were then classified and clustered into their respective protein classes by mapping them into the STRING classification system. The PPI network of all upregulated proteins in the HTyr-OL treated cells is presented in Figure 9. A total of 17 nodes and 13 edges were identified in the PPI network, and two significant interactions between DEPs were generated from k-means clustering analysis. Both networks also revealed that the DEPs with similar functional roles were grouped into a cluster, and inter-cluster interaction was displayed. The highly connected first cluster (in red in Figure 9) was made up of "Histone Fold" proteins (e.g., Core histone macro-H2A.1, H2AFY; Histone cluster 1 H4 family member f, HIST1H4F; Histone cluster 2 h2a family member c, HIST2H2AC; Histone cluster 2 h2b family member e, HIST2H2BE; Histone cluster 2 H3 pseudogene 2, HIST2H3PS2). The second cluster consisted of proteins involved in apoptosis and the response to oxidative stress, such as BAG3, SQSTM1, HMOX1, and Sulfiredoxin-1 (SRXN1). The remaining un-clustered proteins were 1,4-Alpha-glucan-branching enzyme (GBE1), HERPUD1, Interferon-related developmental regulator 1 (IFRD1), Neuro secretory protein VGF (VGF), AN1-type zinc finger protein 5 (ZFAND5), and Protein Niban 1 (FAM129A).
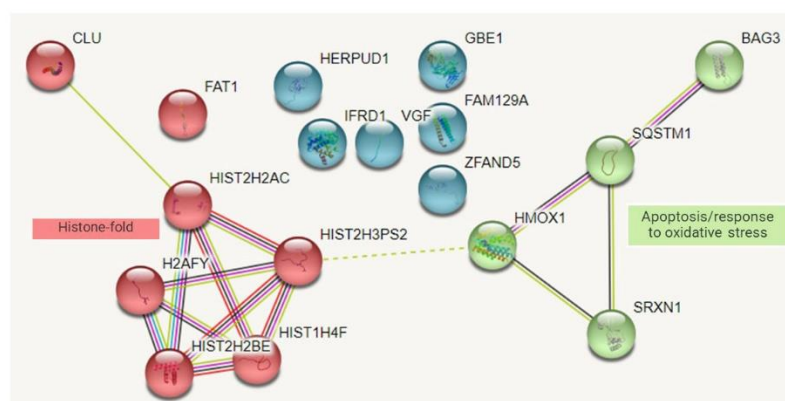
Figure 9. Protein–protein interaction (PPI) network of DEPs identified in HTyr-OL that describes the node proteins, wherein nodes in the same cluster are shown in the same color. The lines connecting the nodes indicate the associations between the proteins. The first cluster "Histone fold" is in red, and the second cluster "Apoptosis and response to oxidative stress" is in green. Proteins in blue are not included in a cluster.

3. Discussion

HTyr-OL is a very interesting compound, having in its chemical structure the catechol moiety of HTyr, which is responsible for a variety of biological activities, linked to the monounsaturated chain of OA, which confers high lipophilicity and bioavailability in the cellular environment.

To investigate the potentiality of HTyr-OL to act on tumoral cell lines, this research was focused on the evaluation of HTyr-OL's in vitro cytotoxicity, anti-proliferative, and apoptotic induction activities against SH-SY5Y human neuroblastoma cells. Its effects were compared to those of HTyr and OA.

For this purpose, HTyr and HTyr-OL were synthesized in our laboratory upon use to obtain samples of high purity, while OA was a commercially available product. HTyr-OL was prepared in a good yield (60%) by treating HTyr with oleyl chloride in DMC. Fresh HTyr was obtained in a moderate yield (40%) by the direct oxidation of tyrosol with IBX in methanol, and the following reductive step was carried out with $Na_2S_2O_4$ in water [45,46]. Both products were purified by flash chromatography.

In our study, the cytotoxic and anti-proliferative assays demonstrated that the activity of HTyr against SH-SY5Y cells was enhanced in its lipophilic derivate HTyr-OL, which showed lower EC_{50} values over the three incubation times considered, as shown in Table 2. SH-SY5Y cells were also investigated by the flow cytometry technique and by Western blot analysis to search for the presence of Annexin V-FITC and Propidium Iodide (PI) staining and caspase-3, respectively, to determine whether the cell death was related to an apoptotic process. Apoptosis is a fundamental mechanism that enables the maintenance of the normal balance between cell death and survival to prevent cancer and other associated diseases [48].

The cytotoxicity induced by HTyr-OL on SH-SY5Y cells was clearly demonstrated to be related to an apoptotic process, with evidence provided by the apoptotic rate of $52.36 \pm 4.31\%$, the presence of active caspase 3, and the clear morphological and ultra-structural changes observed, namely cell shrinking, the presence of rounded cells whose surfaces was characterized by apoptotic blebs [49].

The obtained results indicated that the anti-proliferative effects induced by HTyr-OL were increased compared with the HTyr and OA-treated cells. Cell growth inhibition by HTyr was demonstrated in several cancer cell lines, such as three colon carcinoma cell lines (HT-29, HCT-116, CT-26) [50]. In mammary adenocarcinoma cells (MCF-7) and in human leukaemia cells (HL-60), HTyr was found to have dose- and time-dependent anti-proliferative activity above 200 μM after 12 h of exposure for MCF-7 and at 100 μM

after 24 h of exposure for HL-60; in both cases, the inhibition of cell growth was observed to be related to the induction of an apoptotic process [51,52].

The induction of apoptosis by HTyr was studied in pancreatic carcinoma cells (MIA PaCa-2) in which an apoptotic rate of 47.17% was reported, correlating with the detection of caspases 3 and 7 [53]. Furthermore, chemopreventive effects of HTyr due to the induction of anti-proliferative and apoptotic activity were observed in human promyelocytic cells (HL60) and in colon adenocarcinoma cells (HT-29 and DLD1) [54–57].

The results of the present study regarding the OA treatments revealed the positivity of Annexin V/IP by flow cytometry, coupled with the absence of cleaved caspase-3 detection by Western blot, confirming the data reported by Zhu and colleagues (2005), who observed an apoptotic process on neuronal cells through an OA-induced caspase-3-independent mechanism [58]. Leist and Jaattela in 2001 proposed the classification of different types of programmed cell deaths including an apoptosis-like process characterized by less compact chromatin condensation, phosphatidylserine exposure and absence of executioner caspase activation [59]. However, the mechanisms of OA-induced cell death are still unclear and should be further investigated, as Carrillo and colleagues (2012) concluded in a review on the antitumor effects of OA [60].

In the present study, the results showed that the anti-proliferative activity of HTyr-OL is due to a mechanism of cell death by apoptosis, an effect that was revealed at doses even four times lower than the doses of HTyr.

Lee Yee Qian et al. (2021) evaluated the activities of a curcumin derivative, demonstrating its potent dose dependent cytotoxicity, and time- and dose-dependent anti-proliferative activity in both U-87 MG and SH-SY5Y cells, performing better than its parent compound, curcumin. The authors, by using a proteomic analysis of these cells following treatment with MS13, found that several common Differential Expressed Proteins (DEPs) are involved in the regulation of specific pathways [61].

In the present study, the DEPs profiles, investigated in Ctrl and HTyr-OL samples by the shotgun proteomic approach, revealed that in the biological process category, the most significantly enriched GO terms annotated by the unique proteins in the two sample groups confirm the antioxidant, antiproliferative, and anti-inflammatory activities of HTyr-OL. Namely, a high percentage of unique Ctrl proteins involved in cellular proliferation pathways, such as "Neuroblast proliferation" (67.55% in Ctrl, 32.45% in HTyr-OL), in the inflammation process such as "Cytokine production involved in inflammatory response" (73.51% in Ctrl; 26.49% in HTyrOL), "Stress-activated MAPK cascade" (89.28% in Ctrl; 10.72% in HTyr-OL), "Stress-activated protein kinase signalling cascade" (90.02% in Ctrl; 9.98% in HTyr-OL) and in antioxidant activity, such as "Cellular response to oxidative stress" (60.05% in Ctrl; 39.95% in HTyr-OL), was found. Moreover, it should be noted that a high percentage of the Ctrl proteins were found to be involved in "Mitotic DNA damage checkpoint signalling" (61.82% in Ctrl; 38.18% in HTyr-OL) and "DNA damage checkpoint signalling" (69.81% in Ctrl; 30.19% in HTyr-OL). This aspect confirmed that DNA damage was more represented in the Ctrl group rather than in the HTyr-OL treated samples, which showed dose- and time-dependent antiproliferative and apoptotic effects.

Among the 220 HTyr-OL proteins, the "induced myeloid leukaemia cell differentiation protein Mcl-1" (MCL1, or its alternative name Bcl-2-like protein 3 (Bcl2-L-3) is involved in the regulation of apoptosis versus cell survival, and in the maintenance of viability but not proliferation. It mediates its effects by interactions with a number of other regulators of apoptosis, and it is implicated in the extrinsic apoptotic signalling pathway in the absence of ligands, and the intrinsic apoptotic signalling pathway in response to DNA damage [62]. Additionally, another protein, Presenilin 1 (PSEN1), is involved in cell proliferation inhibition and apoptosis induction by suppressing phosphatidylinositol 3-kinase/protein kinase B (PI3K/AKT) signalling [63–65].

Specifically, among the upregulated proteins, BAG family molecular chaperone regulator 3 (BAG3) is included. This is involved in the extrinsic apoptotic signaling pathway via death domain receptors [GO:0008625], which gather molecular signals conveyed from

the cell surface to trigger the apoptotic death of a cell. The pathway starts with a ligand binding to a death domain receptor on the cell surface, and ends when the execution phase of apoptosis is triggered. Similarly, Heme oxygenase 1 (HMOX1), Clusterin (CLU), and Homocysteine-responsive endoplasmic reticulum-resident ubiquitin-like domain member 1 protein (HERPUD1) are connected to the intrinsic apoptotic signaling pathway in response to DNA damage [GO:0008630]. Such a pathway is induced by the detection of DNA damage and ends when the execution phase of apoptosis is triggered. In the positive regulation of the apoptotic process, the Sequestosome-1 (SQSTM1) protein is also implicated.

Conversely, among downregulated proteins, Myc-associated zinc finger protein (MAZ) is linked with the negative regulation of the apoptotic signaling pathway [GO:2001234], including any process that stops, prevents, or reduces the frequency, rate, or extent of the apoptotic signaling pathway. Another downregulated HTyr-OL protein is Histone deacetylase 1 (HDAC1), which is associated with the positive regulation of cell population proliferation [GO:0008284].

A histone fold is a structurally conserved motif found near the C-terminus in every core histone sequence in a histone octamer, and is responsible for the binding of histones into heterodimers. Histone-fold proteins are important in DNA damage repair [66].

4. Materials and Methods

4.1. Chemical and Reagents

Reagents, chemicals (including OA), solvents, silica gel 60 F254 plates, and silica gel 60 were furnished by Merck (Milan, Italy). HTyr and HTyr-OL were synthesized in laboratory as reported in Section 4.3 [45]. IBX was prepared upon use according to the procedure described in the literature [67].

4.2. Instrumentation

A 400 MHz Nuclear Magnetic Resonance Spectrometer Advance-III Bruker (Munich, Germany) was used to record the spectra (^{1}H NMR, ^{13}C NMR) of all compounds. Chemical shifts were expressed in parts per million (δ scale). Each sample (25–30 mg) was solubilized in chloroform-d3 or methanol-d4 (0.5 mL).

The absorbance of solubilized, purple-colored formazan product by MTT assay was read by a Tecan Sunrise™ UV-vis spectrophotometer at 595 nm. The emitted fluorescence of cells was stained with an Annexin V-FITC conjugate and PI, and was analysed using a flow cytometer (BD Accuri C6 Plus, BD Italy S.p.A, Milan, Italy). The samples for scanning electron microscopy analysis were dried with a critical point dryer using CO2 in a Balzers Union CPD 020, coated with gold in a Balzers MED 010 unit, and observed under a JEOL JSM 5200 electron microscope (Jeol Ltd., Tokyo, Japan).

LC-MS/MS analyses were performed using Q-Exactive HF-X UHPLC Nano mass spectrometer (Thermo Scientific, Waltham, MA, USA). The peptide separation was carried out at 37 °C using a peptide PepMap RSLC C18 column, 75 μm × 15 mm, 2 μm, 100 Å (Thermo Scientific, Waltham, MA, USA) at a flow rate of 0.300 μL/min.

4.3. Synthesis of HTyr and HTyr-OL

Tyrosol (138 mg, 1.0 mmol) was solubilized in methanol (10 mL) and kept at -10 °C. Then, IBX (403 mg, 1.44 mmol) was added under stirring. After 2 h, the mixture was placed at room temperature; then, water (3.5 mL) and $Na_2S_2O_4$ (348 mg, 2.0 mmol) were added. After 1 h, the methanol was evaporated under vacuum. The aqueous residue was extracted with ethyl acetate (3 × 15 mL). The organic phases were washed with a saturated solution of $NaHCO_3$ (3.0 mL) and then with a saturated solution of NaCl (3.0 mL). Finally, the extracts were dried over Na_2SO_4 and filtered. After evaporation of the solvent, the reaction crude was purified by chromatographic column on silica gel (eluent in gradient: CH_2Cl_2/CH_3OH from 9.9/0.1 to 9.5/0.5). The isolated product was characterized by ^{1}H and ^{13}C NMR and identified as HTyr (yellow oil, yield: 40%). NMR spectra were according to those reported in the literature [45].

For the synthesis of HTyr-OL, HTyr (154 mg, 1.0 mmol) was solubilized in DMC (3.0 mL) at room temperature. Then, oleyl chloride was added (361 mg, 1.2 mmol) and the mixture was kept under stirring. After 24 h, DMC was evaporated under vacuum and the residue was solubilized with ethyl acetate (20 mL); then, a saturated solution of NaCl was added (10 mL). After the extraction with ethyl acetate (3 × 20 mL), the combined organic phases were washed with a saturated solution of NaCl (20 mL), dried over Na_2SO_4, and filtered. After evaporation of the solvent, the reaction crude was purified by chromatographic column on silica gel (eluent in gradient: CH_2Cl_2/CH_3OH from 9.8/0.2 to 9.0/1.0). The isolated product was characterized by ^{1}H and ^{13}C NMR and identified as HTyr-OL (colourless oil, yield: 60%) by comparison with the literature data [31,43].

4.4. Cell Culturing

To evaluate the effect of HTyr-OL, HTyr and OA on cell viability, two different cell lines, human neuroblastoma cells (SH-SY5Y, ATCC® CRL-2266) and normal breast epithelial cell (MCF10A. ATCC® CRL-10317™) were used. The SH-SY5Y cells were cultured in DMEM F-12 supplemented with 10% Fetal Bovine Serum (FBS), 2 mM glutamine and 100 U penicillin/0.1 mg/mL streptomycin. The MCF10A cells were maintained in DMEM F-12 supplemented with 100 ng/mL cholera toxin, 20 ng/mL epidermal growth factor (EGF), 0.01 mg/mL insulin, 500 ng/mL hydrocortisone, 5% Horse Serum (HS), 2 mM glutamine and 100 U penicillin/0.1 mg/mL streptomycin; before being seeded for the viability assay, the culture medium was deprived of EGF and the HS was reduced to 2%. All the cell lines were maintained at 37 °C in a humidified 5% CO_2 condition. All experiments were performed with the cells in their logarithmic growth phase.

4.5. Cytotoxicity and Anti-Proliferative Assay

The cytotoxicity and anti-proliferative activities were performed using the MTT assay, as described by Ovidi et al., 2020 [68]. The cells were seeded in 96 flat-bottomed tissue culture plate at seeding concentrations of 2×10^5 cells/mL for SH-SY5Y cells, and 1×10^5 cells/mL for the MCF10A cells. The plates were incubated in a humidified incubator with 5% CO_2 at 37° C for 24 h to allow the cells to attach to the bottom of the wells. Subsequently, 10 two-fold different concentrations were added to the media, from 200 to 0.39 μM of HTyr-OL, HTyr, and OA. DMSO was used as solvent control and vinblastine as positive control. The cells were treated for 72 h for the dose-dependent cytotoxic activity and for 24, 48, and 72 h for the dose and time-dependent anti-proliferative activity. Following each treatment, the media containing the compounds were aspirated and 100 mL of 0.5 mg/mL of MTT in culture medium was added. After 3 h, the MTT solution in each well was removed, and 100 mL of DMSO was added to solubilize the purple-coloured formazan product. The absorbance was read at 595 nm using a microplate reader. The absorbance reading was corrected to background absorbance, and average reading was taken from three independent experiments. The cell viability in percentage was calculated as follows:

$$\text{Cell viability \%} = \frac{\text{Average absorbance of treated cells}}{\text{Average absorbance of untreated cells (Ctrl)}} \times 100$$

The results were analysed using GraphPad Prism version 8.0.2 for Windows (GraphPad Software, La Jolla, CA, USA). The half-maximal concentration (EC_{50}) for each biological replicate was determined using a constructed log–response curve. Overall EC_{50} was calculated from three independent biological replicates.

4.6. Apoptosis Detection by Flow Cytometry

Annexin V-FITC and PI apoptosis kit (eBioscience™) was used to perform the apoptosis detection. A total of 5×10^5 SH-SY5Y cells /mL were seeded into a six well plate and, after 24 h of incubation, they were treated with HTyr-OL, HTyr and OA at their respective EC_{50} values. Cells grown in media containing DMSO 0.001%, corresponding to the higher percentage applied, were used as solvent control (Ctrl), and cells treated with vinblastine

were used as apoptotic control (VBL). Cells emitting fluorescence were analysed by flow cytometry after 24 h of treatment; the cells were stained with Annexin V-FITC conjugate and propidium iodide. The population plots (dot plot), obtained by acquiring 1×10^4 events of each sample, were used to define the percentage of live cells (L), early apoptotic cells (EA), late apoptotic cells (LA), and necrotic cells (N), on the basis of the florescent signal emitted by each individual event in reference to the axes; Annexin V-FITC green fluorescence in abscissa, vs. PE red fluorescence in ordinate. The experiments were repeated three times.

4.7. Scanning Electron Microscopy

For scanning electron microscope analysis, SH-SY5Y cells were seeded at a density of 3×10^5 cells/mL on a six-well plate and incubated for 24 h under appropriate culture conditions. After treatment with EC_{50} concentrations of each compound tested (VBL and Ctrl were also added as positive and negative controls, respectively) for 24 h, the cells were collected in tubes, washed with PBS and fixed with 4% paraformaldehyde and 5% glutaraldehyde, pH 7.2, in 0.1 M cacodylate buffer for 1 h at 4 °C [69]. After rinsing the samples in the same buffer, they were post-fixed in 1% osmium tetroxide in a cacodylate buffer for 1 h at 4 °C. After the samples were washed twice in the same buffer, they were dehydrated in a graded ethanol series. The samples were then dried with a critical point dryer using CO_2 in a Balzers Union CPD 020, coated with gold in a Balzers MED 010 unit and observed under a JEOL JSM 5200 electron microscope (Jeol Ltd., Tokyo, Japan).

4.8. Detection of Caspase-3 Activated by Western Blot

SH-SY5Y cells were seeded at 1×10^6 cells/mL density into a Petri dish and incubated for 24 h. After treatments with HTyr, HTyr-OL, OA, and vinblastine at their respective EC_{50} concentrations, cells were lysed with NP40 buffer on ice for 30 min. Protein concentrations were determined by the Bradford test. Samples were run on a 10% SDS-PAGE and then electrotransferred onto a pure nitrocellulose membrane (0.45 µm). The membrane was blocked with 5% bovine serum albumin and immunoblotted with cleaved caspase-3 rabbit mAb and β-actin mouse mAb (Cell Signaling Technology Europe B.V., Leiden, The Netherlands). Anti-rabbit IgG (H + L) and anti-mouse IgG (H + L) HRP conjugate antibodies (Promega, Madison, WI, USA) were used to detect the corresponding bands by acquiring images by ChemiDoc XRS+ System (Bio Rad, Segrate, Italy) [70]. Acquired pictures were quantitatively evaluated using the ImageJ program version, ImageJ 1.48v-Wayne Rasband, National Institute of Health, Bethesda, MD, USA.

4.9. Statystical Analysis

The data from three independent experiments on cytotoxicity, anti-proliferative activity, and apoptosis rate obtained by flow cytometry were used and expressed as means ± SD. Statistical analysis was performed using one-way ANOVA test with Stat-Plus software (AnalystSoft VC 2009, Walnut, CA, USA), with the threshold of significance set at *p*-value < 0.05.

4.10. Proteomic Analysis

4.10.1. Preparation of Cell Culture Samples

Cells lysis of SH-SY5Y human neuroblastoma cell was performed using a solution of 1% NP40. The proteins were quantified using BCA assay following manufacturers' instructions. A total of 100 µg of total proteins for each sample was reduced with dithiothreitol (DTT), and consequently alkylated with iodoacetamide (IAA). Then, protein precipitation was performed using a solution of chloroform/methanol (1:4). The protein pellet was resuspended in a solution of 6 M urea. Digestion was performed by adding trypsin (enzyme-to-protein ratio of 1:50) and incubated at 37 °C overnight. After trypsin digestion, all reaction mixtures were acidified with 1% FA in order to inhibit any remaining enzyme activity

4.10.2. Proteomic Analysis

Using OASIS cartridges (Waters), digested samples were desalted, brought to dryness, and reconstituted in 0.1% formic acid in water in order to obtain a concentration of 1 ug/ul. LC-MS/MS analyses were performed using Q Exactive™ HF-X mass spectrometer (Thermo Scientific). Peptide separation was carried out at 35 °C using a PepMap TM RSLC C18 column, 75 μm × 50 cm, 2 μm, and 100 Å at a flow rate of 250 nL/min (Thermo Scientific). The mobile phases A and B used for the analysis were 0.1% formic acid in water and 0.1% formic acid in 80% acetonitrile, respectively. The gradient started with 5% of B, which was kept constant for 5 min. Then, the organic phase was increased up to 36% in 135 min and later was raised up to 90%, kept constant for 11 min and then returned to the initial conditions. These experiments were performed using a data dependent acquisition (DDA) setting to select the "top twelve" most-abundant ions for MS/MS analysis. Proteomic analysis was performed using a Label Free Quantification (LFQ) method. Protein identification was performed using Proteome Discoverer 2.5 (Thermo Scientific) and Sequest algorithm. The peptide spectra were matched against Homo sapiens database downloaded from Uniprot (total proteins: 20,626). The analysis was based on at least two unique peptides with a minimum length of seven amino acids and a false discovery rate of 0.01, which was applied to both peptide and protein levels.

4.10.3. Bioinformatics Analysis

For a functional annotation analysis, the protein identifiers were associated to their related Gene Ontology (GO) terms [71], overcoming the redundancy in terminology for "molecular function", "biological process", and "cellular component" [72]. A p-value < 0.05 was used as a threshold to show over-representation of a specific GO term. FunRich 3.1.3 [73] and ClueGO v2.5.6 (Cytoscape plugin) [74] were applied in this study for Venn diagram representations, for confirming GO results and for a graphical description of enrichment and network analysis. String version 11.0 was used to verify the shell of interactors of specific proteins [75]. The default peak-picking settings were used to process the raw MS files in MaxQuant [76] (version 1.6.1.0) and its integrated search engine Andromeda [77]. MaxQuant automatically aligned the runs. Perseus (version 1.6.1.1) was successively employed for processing of MaxQuant result files. The Label Free Quantification (LFQ) intensities of proteins were imported and transformed to logarithmic scale with base two. The missing values were replaced (imputed) by random numbers drawn from a normal distribution of 1.8 standard deviation down shift and with a width of 0.3 of each sample. The protein quantification and calculation of statistical significance was carried out using two-tailed Student's t-test and error correction (p-value < 0.05) with the method of Benjamini–Hochberg. Moreover, a volcano plot, showing a summary distribution of differentially expressed proteins (DEPs) between Control (Ctrl) and Hydroxytyrosol oleate (HTyr-OL) samples, was calculated. The volcano plot is an easy-to-interpret scatter plot that arranges values along dimensions of biological (difference Ctrl and HTyr-OL) and statistical (log10 p-value) significance. The proteins located on the upper left region and the upper right region (S0 = 2, FDR < 0.05) are differentially expressed.

5. Conclusions

HTyr-OL is a lipophilic HTyr derivative found in EVOO and olive oil by-products that can be synthesized in the laboratory with a good yield and high degree purity. It appears as a potential bioactive compound showing the catecholic moiety of HTyr combined with the monounsaturated chain of OA. Despite this potentiality, to date, HTyr-OL's biological activities have been rarely studied. Due to this gap in the literature, this study, for the first time, evaluated and demonstrated the in vitro cytotoxic, anti-proliferative, and apoptotic inducing activity of HTyr-OL against human SH-SY5Y neuroblastoma cells. Flow cytometry, Western blot and electron microscopy analyses showed that the biological activity of HTyr-OL is caused by a mechanism of cell death by apoptosis, an effect revealed at doses even four times lower than those of HTyr. Proteomic analysis supported the experimental

evidence through the identification of the downregulation of cell proliferation and the up-regulation of the extrinsic apoptotic signaling pathway, demonstrating the potential role of HTyr-OL as a chemopreventive agent.

References

1. Bernardini, S.; Tiezzi, A.; Laghezza Masci, V.; Ovidi, E. Natural products for human health: An historical overview of the drug discovery approaches. *Nat. Prod. Res.* **2018**, *32*, 1926–1950. [CrossRef] [PubMed]
2. Fridlender, M.; Kapulnik, Y.; Koltai, H. Plant derived substances with anti-cancer activity: From folklore to practice. *Front. Plant Sci.* **2015**, *6*, 799. [CrossRef] [PubMed]
3. Lichota, A.; Gwozdzinski, K. Anticancer Activity of Natural Compounds from Plant and Marine Environment. *Int. J. Mol. Sci.* **2018**, *19*, 3533. [CrossRef] [PubMed]
4. Najmi, A.; Javed, S.A.; Al Bratty, M.; Alhazmi, H.A. Modern Approaches in the Discovery and Development of Plant-Based Natural Products and Their Analogues as Potential Therapeutic Agents. *Molecules* **2022**, *27*, 349. [CrossRef] [PubMed]
5. Schwingshackl, L.; Morze, J.; Hoffmann, G. Mediterranean diet and health status: Active ingredients and pharmacological mechanisms. *Br. J. Pharmacol.* **2020**, *177*, 1241–1257. [CrossRef]
6. Bonofiglio, D. Mediterranean diet and physical activity as healthy lifestyles for human health. *Nutrients* **2022**, *14*, 2514. [CrossRef]
7. Cory, H.; Passarelli, S.; Szeto, J.; Tamez, M.; Mattei, J. The role of polyphenols in human health and food systems: A mini-review. *Front. Nutr.* **2018**, *5*, 87. [CrossRef]
8. Santos-Buelga, C.; Gonzalez-Manzano, S.; Gonzalez-Paramas, A.M. Wine, polyphenols, and mediterranean diets. What else is there to say? *Molecules* **2021**, *26*, 5537. [CrossRef]
9. Gambacorta, A.; Tofani, D.; Bernini, R.; Migliorini, A. High yielding preparation of a stable precursor of hydroxytyrosol by total synthesis and from the natural glucoside oleuropein. *J. Agric. Food Chem.* **2007**, *55*, 3386–3391. [CrossRef]
10. Faustino, M.; Veiga, M.; Sousa, P.; Costa, E.M.; Silva, S.; Pintado, M. Agro-food byproducts as a new source of natural food sdditives. *Molecules* **2019**, *24*, 1056. [CrossRef]
11. Romani, A.; Pinelli, P.; Ieri, F.; Bernini, R. Sustainability, innovation and green chemistry in the production and valorization of phenolic extracts from *Olea europaea* L. *Sustainability* **2016**, *8*, 1002. [CrossRef]
12. Luzi, F.; Pannucci, E.; Clemente, M.; Grande, E.; Urciuoli, S.; Romani, A.; Torre, L.; Puglia, D.; Bernini, R.; Santi, L. Hydroxytyrosol and oleuropein-enriched extracts obtained from olive oil wastes and by-products as active antioxidant ingredients for poly-(vinyl alcohol)-based films. *Molecules* **2021**, *26*, 2104. [CrossRef] [PubMed]
13. Aunon-Calles, D.; Giordano, E.; Bohnenberger, S.; Visioli, F. Hydroxytyrosol is not genotoxic in vitro. *Pharmacol. Res.* **2013**, *74*, 87–93. [CrossRef] [PubMed]

14. Aunon-Calles, D.; Canut, L.; Visioli, F. Toxicological evaluation of pure hydroxytyrosol. *Food Chem. Toxicol.* **2013**, *55*, 408–504. [CrossRef]

15. Markovic, A.K.; Toric, J.; Barbaric, M.; Brala, C.J. Hydroxytyrosol, tyrosol and derivatives and their potential effects on human health. *Molecules* **2019**, *24*, 2001. [CrossRef]

16. Fuccelli, R.; Fabiani, R.; Rosignoli, P. Hydroxytyrosol exerts antinflammatory and antioxidant activities in a mouse model of systemic inflammation. *Molecules* **2018**, *23*, 3212. [CrossRef]

17. Leo, M.; Muccillo, L.; Dugo, L.; Bernini, R.; Santi, L.; Sabatino, L. Polyphenols extracts from oil production waste products (OPWPs) reduce cell viability and exert anti-inflammatory activity via PPAγ induction in colorectal cancer cells. *Antioxidants* **2022**, *11*, 624. [CrossRef]

18. Fabiani, R.; Rosignoli, P.; De Bartolomeo, A.; Fuccelli, R.; Morozzi, G. Inhibition of cell cycle progression by hydroxytyrosol is associated with upregulation of cyclindependent protein kinase inhibitors p21(WAF1/Cip1) and p27(Kip1) and with induction of differentiation in HL60 cells. *J. Nutr.* **2008**, *138*, 42–48. [CrossRef]

19. Bernini, R.; Merendino, N.; Romani, A.; Velotti, F. Naturally occurring hydroxytyrosol: Synthesis and anticancer potential. *Curr. Med. Chem.* **2013**, *20*, 655–670. [CrossRef]

20. Bernini, R.; Gilardini Montani, M.S.; Merendino, N.; Romani, A.; Velotti, F. Hydroxytyrosol-derived compounds: A basis for the creation of new pharmacological agents for cancer prevention and therapy. *J. Med. Chem.* **2015**, *58*, 9089–9107. [CrossRef]

21. Hamden, K.; Allouche, N.; Jouadi, B.; El-Fazaa, S.; Gharbi, N.; Carreau, S.; Damak, M.; Elfeki, A. Inhibitory action of purified hydroxytyrosol from stored olive mill waste on intestinal disaccharidases and lipase activities and pancreatic toxicity in diabetic rats. *Food Sci. Biotechnol.* **2010**, *19*, 439–447. [CrossRef]

22. Covas, M.I.; Nyyssonen, K.; Poulsen, H.E.; Kaikkonen, J.; Zunft, H.J.; Kiesewetter, H.; Gaddi, A.; de la Torre, R.; Mursu, J.; Baumler, H.; et al. The effect of polyphenols in olive oil on heart disease risk factors: A randomized trial. *Ann. Intern. Med.* **2006**, *145*, 333–341. [CrossRef]

23. Gonzalez-Santiago, M.; Martin-Bautista, E.; Carrero, J.J.; Fonolla, J.; Baro, L.; Bartolomé, M.V.; Gil-Loyzaga, P.; López-Huertas, E. One-month administration of hydroxytyrosol a phenolic antioxidant present in olive oil to hyperlipemic rabbits improves blood lipid profile antioxidant status and reduces atherosclerosis development. *Atherosclerosis* **2006**, *188*, 35–42. [CrossRef]

24. González-Correa, J.A.; Navas, M.D.; Lopez-Villodres, J.A.; Trujillo, M.; Espartero, J.L.; de La Cruz, J.P. Neuroprotective effect of hydroxytyrosol and hydroxytyrosol acetate in rat brain slices subjected to hypoxia-reoxygenation. *Neurosci. Lett.* **2008**, *446*, 143–146. [CrossRef]

25. Rodriguez-Morato, J.; Xicota, L.; Fito, M.; Farré, M.; Dierssen, M.; de La Torre, R. Potential role of olive oil phenolic compounds in the prevention of neurodegenerative diseases. *Molecules* **2015**, *20*, 4655–4680. [CrossRef]

26. D'Andrea, G.; Ceccarelli, M.; Bernini, R.; Clemente, M.; Santi, L.; Caruso, C.; Micheli, L.; Tirone, F. Hydroxytyrosol stimulates neurogenesis in aged dentate gyrus by enhancing stem and progenitor cell proliferation and neuron survival. *FASEB J.* **2020**, *34*, 4512–4526. [CrossRef]

27. EFSA. Scientific Opinion on the Substantiation of Health Claims Related to Polyphenols in Olive and Protection of LDL Particles from Oxidative Damage (ID 1333,1638, 1639, 1696, 2865), Maintenance of Normal Blood HDL Cholesterol Concentrations (ID 1639), Maintenance of Normal Blood Pressure (ID 3781), "Anti-Inflammatory Properties" (ID 1882), "Contributes to the Upper Respiratory Tract Health" (ID 3468), "Can Help to Maintain a Normal Function of Gastrointestinal Tract" (3779), and "Contributes to Body Defences against External Agents" (ID 3467) Pursuant to Article 13 of Regulation (EC) No 1924/2006. Available online: https://www.efsa.europa.eu/en/efsajournal/pub/2033 (accessed on 5 August 2020).

28. Robles-Almazan, M.; Pulido-Moran, M.; Moreno-Fernandez, J.; Ranirez-Tortosa, C.; Rodriguez-Garcia, C.; Quiles, J.L.; Ramirez-Tortosa, M.C. Hydroxytyrosol: Bioavailability, toxicity, and clinical applications. *Food Res. Int.* **2018**, *105*, 654–667. [CrossRef] [PubMed]

29. Bouallagui, Z.; Bouaziz, M.; Lassoued, S.; Engasser, J.M.; Ghoul, M.; Sayadi, S. Hydroxytyrosol acyl esters: Biosynthesis and activities. *Appl. Biochem. Biotech.* **2011**, *163*, 592–599. [CrossRef] [PubMed]

30. Trujillo, M.; Gallardo, E.; Madrona, A.; Bravo, L.; Sarria, B.; Gonzalez-Correa, J.A.; Espartero, J.L. Synthesis and antioxidant activity of nitrohydroxytyrosol and its acyl derivatives. *J. Agric. Food Chem.* **2014**, *62*, 10297–10303. [CrossRef]

31. Bernini, R.; Barontini, M.; Cis, V.; Carastro, I.; Tofani, D.; Chiodo, R.A.; Lupattelli, P.; Incerpi, S. Synthesis and evaluation of the antioxidant activity of lipophilic phenethyl trifluoroacetate esters by in vitro ABTS, DPPH and in cell-culture DCF assays. *Molecules* **2018**, *23*, 208. [CrossRef] [PubMed]

32. Bernini, R.; Carastro, I.; Santoni, F.; Clemente, M. Synthesis of lipophilic esters of tyrosol, homovanillyl alcohol and hydroxytyrosol. *Antioxidants* **2019**, *8*, 174. [CrossRef]

33. Pereira-Caro, G.; Madrona, A.; Bravo, L.; Cert, A.; Espartero, J.L.; Alcudia, F.; Mateos, R. Antioxidant activity evaluation of alkyl hydroxytyrosyl ethers, a new class of hydroxytyrosol derivatives. *Food Chem.* **2009**, *115*, 86–91. [CrossRef]

34. Procopio, A.; Celia, C.; Nardi, M.; Oliverio, M.; Paolino, D.; Sindona, G. Lipophilic hydroxytyrosol esters: Fatty acid conjugates for potential topical administration. *J. Nat. Prod.* **2011**, *74*, 2377–2381. [CrossRef]

35. Calderon-Montano, J.M.; Madrona, A.; Burgos-Moron, E.; Orta, M.L.; Mateos, S.; Espartero, J.L.; Lopez-Lazaro, M. Selective cytotoxic activity of new lipophilic hydroxytyrosol alkyl ether derivatives. *J. Agric. Food Chem.* **2013**, *61*, 5046–5053. [CrossRef]

36. Bianco, A.; Coccioli, F.; Guiso, M.; Marra, C. The occurrence in olive oil of a new class of phenolic compounds: Hydroxy-isochromans. *Food Chem.* **2002**, *77*, 405–411. [CrossRef]

37. Bernini, R.; Crisante, F.; Fabrizi, G.; Gentili, P. Convenient synthesis of 1-aryl-dihydroxyisochromans exhibiting antioxidant activity. *Curr. Org. Chem.* **2012**, *16*, 1051–1057. [CrossRef]

38. Roma, E.; Mattoni, E.; Lupattelli, P.; Moeini, S.S.; Gasperi, T.; Bernini, R.; Incerpi, S.; Tofani, D. New dihydroxytyrosyl esters from dicarboxylic acids. Synthesis and evaluation of the antioxidant activity in vitro (ABTS) and in cell-cultures (DCF assay). *Molecules* **2020**, *25*, 3135. [CrossRef] [PubMed]

39. Bovicelli, P.; Bernini, R.; Antonioletti, R.; Mincione, E. Selective halogenation of flavanones. *Tetrahedron Lett.* **2002**, *43*, 5563–5567. [CrossRef]

40. Plastina, P.; Benincasa, C.; Perri, E.; Fazio, A.; Augimeri, G.; Poland, M.; Witkamp, R.; Meijerink, J. Identification of hydroxytyrosyl oleate, a derivative of hydroxytyrosol with anti-inflammatory properties, in olive oil by-products. *Food Chem.* **2019**, *279*, 105–113. [CrossRef]

41. Bernini, R.; Carastro, I.; Palmini, G.; Tanini, A.; Zonefrati, R.; Pinelli, P.; Brandi, M.L.; Romani, A. Lipophilization of hydroxytyrosol-enriched fractions from *Olea europaea* L. byproducts and evaluation of the in vitro effects on a model of colorectal cancer cells. *J. Agric. Food Chem.* **2017**, *65*, 6506–6512. [CrossRef] [PubMed]

42. Benincasa, C.; La Torre, C.; Plastina, P.; Fazio, A.; Perri, E.; Caroleo, M.C.; Gallelli, R.; Cannataro, R.; Cione, E. Hydroxytyrosyl oleate: Improved extraction procedure from olive oil and by-products, and in vitro antioxidant and skin regenerative properties. *Antioxidants* **2019**, *8*, 233. [CrossRef]

43. Caroleo, M.C.; Plastina, P.; Fazio, A.; La Torre, C.; Manetti, F. Olive oil lipophenols induce insulin secretion in 832/13 b-cell models. *Pharmaceuticals* **2021**, *13*, 1085. [CrossRef]

44. Gupta, A.; Dwivedi, T. A simplified overview of World Health. Organization classification update of central nervous system tumors 2016. *J. Neurosci. Rural Pract.* **2017**, *8*, 629–641. [CrossRef] [PubMed]

45. Bernini, R.; Mincione, E.; Barontini, M.; Crisante, F. Convenient synthesis of hydroxytyrosol and its lipophilic derivatives from tyrosol or homovanillyl alcohol. *J. Agric. Food Chem.* **2008**, *56*, 8897–8904. [CrossRef]

46. Bernini, R.; Fabrizi, G.; Pouysegu, L.; Deffieux, D.; Quideau, S. Synthesis of biologically active catecholic compounds via ortho-selective oxygenation of phenolic compounds using hypervalent iodine(V) reagents. *Curr. Org. Synth.* **2012**, *9*, 650–669. [CrossRef]

47. The UniProt Consortium, UniProt: The universal protein knowledgebase in 2021. *Nucleic Acids Res.* **2021**, *49*, 480–489. [CrossRef] [PubMed]

48. Elmore, S. Apoptosis: A Review of Programmed Cell Death. *Toxicol. Pathol.* **2007**, *35*, 495–516. [CrossRef] [PubMed]

49. Saraste, A.; Pulkki, K. Morphologic and biochemical hallmarks of apoptosis. *Cardiovasc. Res.* **2000**, *45*, 528–537. [CrossRef] [PubMed]

50. Bassani, B.; Rossi, T.; De Stefano, D.; Pizzichini, D.; Corradino, P.; Macrì, N.; Noonan, D.M.; Albini, A.; Bruno, A. Potential chemopreventive activities of a polyphenol rich purified extract from olive mill wastewater on colon cancer cells. *J. Funct. Foods* **2016**, *27*, 236–248. [CrossRef]

51. Han, J.; Talorete, T.P.N.; Yamada, P.; Isoda, H. Anti-proliferative and apoptotic effects of oleuropein and hydroxytyrosol on human breast cancer MCF-7 cells. *Cytotechnology* **2009**, *59*, 45–53. [CrossRef] [PubMed]

52. Ragione, F.D.; Cucciolla, V.; Borriello, A.; Pietra, V.D.; Pontoni, G.; Racioppi, L.; Manna, C.; Galletti, P.; Zappia, V. Hydroxytyrosol, a natural molecule occurring in olive oil, induces cytochrome c-dependent apoptosis. *Biochem. Biophys. Res. Commun.* **2000**, *278*, 733–739. [CrossRef]

53. Goldsmith, C.D.; Bond, D.R.; Jankowski, H.; Weidenhofer, J.; Stathopoulos, C.E.; Roach, P.D.; Scarlett, C.J. The Olive Biophenols Oleuropein and Hydroxytyrosol Selectively Reduce Proliferation, Influence the Cell Cycle, and Induce Apoptosis in Pancreatic Cancer Cells. *Int. J. Mol. Sci.* **2018**, *19*, 1937. [CrossRef] [PubMed]

54. Corona, G.; Deiana, M.; Incani, A.; Vauzour, D.; Dessì, M.A.; Spencer, J.P. Hydroxytyrosol inhibits the proliferation of human colon adenocarcinoma cells through inhibition of ERK1/2 and cyclin D1. *Mol. Nutr. Food Res.* **2009**, *53*, 897–903. [CrossRef]

55. Terzuoli, E.; Donnini, S.; Giachetti, A.; Iñiguez, M.A.; Fresno, M.; Melillo, G.; Ziche, M. Inhibition of hypoxia inducible factor-1alpha by dihydroxyphenylethanol, a product from olive oil, blocks microsomal prostaglandin-E synthase-1/vascular endothelial growth factor expression and reduces tumor angiogenesis. *Clin. Cancer Res.* **2010**, *16*, 4207–4216. [CrossRef] [PubMed]

56. Sun, L.; Luo, C.; Liu, J. Hydroxytyrosol induces apoptosis in human colon cancer cells through ROS generation. *Food Funct.* **2014**, *5*, 1909–1914. [CrossRef] [PubMed]

57. Achmon, Y.; Fishman, A. The antioxidant hydroxytyrosol: Biotechnological production challenges and opportunities. *Appl. Microbiol. Biotechnol.* **2015**, *99*, 1119–1130. [CrossRef] [PubMed]

58. Zhu, Y.; Schwarz, S.; Ahlemeyer, B.; Grzeschik, S.; Klumpp, S.; Krieglstein, J. OA causes apoptosis and dephosphorylates Bad. *Neurochem. Int.* **2005**, *46*, 127–135. [CrossRef]

59. Leist, M.; Jäättelä, M. Four deaths and a funeral: From caspases to alternative mechanisms. *Nat. Rev. Mol. Cell Biol.* **2001**, *2*, 589–598. [CrossRef]

60. Carrillo, C.; Cavia, M.M.; Alonso-Torre, S.R. Antitumor effect of oleic acid; mechanisms of action. A review. *Nutr. Hosp.* **2012**, *27*, 1860–1865. [CrossRef] [PubMed]

61. Lee, Y.Q.; Rajadurai, P.; Abas, F.; Othman, I.; Naidu, R. Proteomic Analysis on Anti-Proliferative and Apoptosis Effects of Curcumin Analog, 1,5-bis(4-Hydroxy-3-Methyoxyphenyl)-1,4-Pentadiene-3-One-Treated Human Glioblastoma and Neuroblastoma Cells. *Front. Mol. Biosci.* **2021**, *8*, 645856. [CrossRef]

62. Maurer, U.; Charvet, C.; Wagman, A.S.; Dejardin, E.; Green, D.R. Glycogen synthase kinase-3 regulates mitochondrial outer membrane permeabilization and apoptosis by destabilization of MCL-1. *Mol. Cell* **2006**, *21*, 749–760. [CrossRef] [PubMed]

63. He, X.Y.; Xu, Y.; Xia, Q.J.; Zhao, X.M.; Li, S.; He, X.Q.; Wang, R.R.; Wang, T.H. Combined Scutellarin and C18H17NO6 Imperils the Survival of Glioma: Partly Associated With the Repression of PSEN1/PI3K-AKT Signaling Axis. *Front. Oncol.* **2021**, *11*, 663262. [CrossRef]

64. Baki, L.; Shioi, J.; Wen, P.; Shao, Z.; Schwarzman, A.; Gama-Sosa, M.; Neve, R.; Robakis, N.K. PS1 activates PI3K thus inhibiting GSK-3 activity and tau overphosphorylation: Effects of FAD mutations. *EMBO J.* **2004**, *23*, 2586–2596. [CrossRef] [PubMed]

65. Tao, L.; Zeng, Y.; Wang, J.; Liu, Z.; Shen, B.; Ge, J.; Liu, Y.; Guo, Y.; Qiu, J. Differential microRNA expression in aristolochic acid-induced upper urothelial tract cancers ex vivo. *Mol. Med. Rep.* **2015**, *12*, 6533–6546. [CrossRef] [PubMed]

66. Mathew, V.; Pauleau, A.L.; Steffen, N.; Bergner, A.; Becker, P.B.; Erhardt, S. The histone-fold protein CHRAC14 influences chromatin composition in response to DNA damage. *Cell Rep.* **2014**, *7*, 321–330. [CrossRef] [PubMed]

67. Frigerio, M.; Santagostino, M.; Sputore, S. A user-friendly entry to 2-iodoxybenzoic acid (IBX). *J. Org. Chem.* **1999**, *64*, 4537–4538. [CrossRef]

68. Ovidi, E.; Laghezza Masci, V.; Garzoli, S.; Gambellini, G.; Keita, S.V.; Zago, D.; Turchetti, G.; Modesti, L.; Tiezzi, A. Antiproliferative properties of *Papaver rhoeas* ovule extracts and derived fractions tested on HL60 Leukemia human cells. *Molecules* **2020**, *25*, 1850. [CrossRef]

69. Karnovsky, M.J. A formaldehyde-glutaraldehyde fixative of high osmolality for use in electron microscopy. *J. Cell Biol.* **1965**, *27*, 137–138.

70. Laghezza Masci, V.; Ovidi, E.; Taddei, A.R.; Turchetti, G.; Tiezzi, A.; Giacomello, P.; Garzoli, S. Apoptotic effects on HL60 human leukaemia cells induced by lavandin essential oil treatment. *Molecules* **2020**, *25*, 538. [CrossRef] [PubMed]

71. Ashburner, M.; Ball, C.A.; Blake, J.A.; Botstein, D.; Butler, H.; Cherry, J.M.; Davis, A.P.; Dolinski, K.; Dwight, S.S.; Eppig, J.T.; et al. Gene ontology: Tool for the unification of biology. The Gene Ontology Consortium. *Nat. Genet.* **2000**, *25*, 25–29. [CrossRef]

72. Rhee, S.Y.; Wood, V.; Dolinski, K.; Draghici, S. Use and misuse of the gene ontology annotations. *Nat. Rev. Genet.* **2008**, *9*, 509–515. [CrossRef]

73. Pathan, M.; Keerthikumar, S.; Chisanga, D.; Alessandro, R.; Ang, C.S.; Askenase, P.; Batagov, A.O.; Benito-Martin, A.; Camussi, G.; Clayton, A.; et al. A novel community driven software for functional enrichment analysis of extracellular vesicles data. *J. Extracell. Vesicles* **2017**, *6*, 1321455. [CrossRef] [PubMed]

74. Bindea, G.; Mlecnik, B.; Hackl, H.; Charoentong, P.; Tosolini, M.; Kirilovsky, A.; Fridman, W.H.; Pagès, F.; Trajanoski, Z.; Galon, J. ClueGO: A Cytoscape plug-in to decipher functionally grouped gene ontology and pathway annotation networks. *Bioinformatics* **2009**, *25*, 1091–1093. [CrossRef] [PubMed]

75. Szklarczyk, D.; Gable, A.L.; Lyon, D.; Junge, A.; Wyder, S.; Huerta-Cepas, J.; Simonovic, M.; Doncheva, N.T.; Morris, J.H.; Bork, P.; et al. STRING v11: Protein-protein association networks with increased coverage, supporting functional discovery in genome-wide experimental datasets. *Nucleic Acids Res.* **2019**, *47*, D607–D613. [CrossRef] [PubMed]

76. Cox, J.; Mann, M. MaxQuant enables high peptide identification rates, individualized p.p.b.-range mass accuracies and proteome-wide protein quantification. *Nat. Biotechnol.* **2008**, *26*, 1367–1372. [CrossRef] [PubMed]

77. Cox, J.; Neuhauser, N.; Michalski, A.; Scheltema, R.A.; Olsen, J.V.; Mann, M. Andromeda: A peptide search engine integrated into the MaxQuant environment. *J. Proteome Res.* **2011**, *10*, 1794–1805. [CrossRef] [PubMed]